J|A|C|S
ARTICLES
Published on Web 03/16/2007

Dehydrogenation of Aromatic Molecules under a Scanning Tunneling Microscope: Pathways and Inelastic Spectroscopy Simulations

Hervé Lesnard,[†] Marie-Laure Bocquet,[†] and Nicolás Lorente[‡,*]

Contribution from the [†]Laboratoire de Chimie, UMR 5182, ENS Lyon, 46 allée d'Italie, 69364 Lyon, France, and [‡]Laboratoire Collisions Agrégats Réactivité, UMR 5589, IRSAMC, Université Paul Sabatier, 31062 Toulouse, France

Received October 18, 2006; E-mail: lorente@irsamc.ups-tlse.fr

Abstract: We have performed a theoretical study on the dehydrogenation of benzene and pyridine molecules on Cu(100) induced by a scanning tunneling microscope (STM). Density functional theory calculations have been used to characterize benzene, pyridine, and different dehydrogenation products. The adiabatic pathways for single and double dehydrogenation have been evaluated with the nudge elastic band method. After identification of the transition states, the analysis of the electronic structure along the reaction pathway yields interesting information on the electronic process that leads to H-scission. The adiabatic barriers show that the formation of double dehydrogenated fragments is difficult and probably beyond reach under the actual experimental conditions. However, nonadiabatic processes cannot be ruled out. Hence, in order to identify the final dehydrogenation products, the inelastic spectra are simulated and compared with the experimental ones. We can then assign phenyl (C_6H_5) and α-pyridil (α-C_5H_4N) as the STM-induced dehydrogenation products of benzene and pyridine, respectively. Our simulations permit us to understand why phenyl, pyridine, and α-pyridil present tunneling-active C−H stretch modes in opposition to benzene.

1. Introduction

The adsorption of organic molecules on metal surfaces is of great relevance to a wide range of systems, from the tuning of self-assembled monolayers to heterogeneous catalysis. For more than two decades, the scanning tunneling microscope (STM) in ultrahigh-vacuum conditions has provided an atomic-scale view of adsorbates on metal surfaces. Recently, STM-induced manipulations have paved the way to unprecedented control of chemical reactions on the atomic scale.[1−4] However, the direct chemical assignment of the observed species is difficult and sometimes impossible, if the analyzed molecular system is largely unkown, especially after a chemical reaction. A new measuring mode of the STM is permitting us to solve this problem.[5] Indeed, inelastic electron tunneling spectroscopy (IETS) with the STM has proved to be a unique chemical probe in determining molecular species and conformations on surfaces.[5−8] In order to analyze the experimental data, density functional theory (DFT) based calculations are becoming a standard tool in IETS interpretations.[9−11] Recently, the identification of the dehydrogenation product of benzene after an STM pulse has been made possible by IETS simulations.[11] Yet, the analysis of the products alone is not sufficient to characterize the reaction, and there is a lot of activity devoted to the evaluation of the actual reaction pathways. The theoretical state-of-the-art is quickly evolving, and DFT has now reached the level of quantitative predictions of reaction barriers.[12] These theoretical advances permit us to have an enhanced insight over the reaction products as well as processes on the atomic scale.

We focus here on STM-induced reactions of benzene and pyridine molecules adsorbed on Cu(100) as schematically represented in Figure 1. These systems have been studied experimentally[13] by transforming the molecules with an STM pulse and by analyzing the initial reactants and final products with constant current STM images as well as IETS. More recent measurements of the dehydrogenation of benzene elaborate on the STM-induced reaction mechanism.[14] Both benzene and pyridine undergo dehydrogenations after tip pulses of the same order of magnitude (2.9−3 V,[13] 2.4 V[14]). This common threshold suggests similar processes. However, it is well-known from previous experimental[15−22] and theoretical studies[23,24] that

[†] ENS Lyon.
[‡] Université Paul Sabatier.

(1) Lee, H. J.; Ho, W. *Science* **1999**, *286*, 1719−1722.
(2) Komeda, T.; Kim, Y.; Kawai, M.; Persson, B. N. J.; Ueba, H. *Science* **2002**, *295*, 2055−2058.
(3) Pascual, J. I.; Lorente, N.; Song, Z.; Conrad, H.; Rust, H.-P. *Nature* **2003**, *423*, 525−528.
(4) Sloan, P. A.; Palmer, R. E. *Nature* **2005**, *434*, 367−371.
(5) Stipe, B. C.; Rezaei, M. A.; Ho, W. *Science* **1998**, *280*, 1732−1735.
(6) Lauhon, L. J.; Ho, W. *Phys. Rev. Lett.* **2000**, *84*, 1527−1530.
(7) Lauhon, L. J.; Ho, W. *Rev. Sci. Instrum. A* **2001**, *72*, 216−223.
(8) Kim, Y.; Komeda, T.; Kawai, M. *Phys. Rev. Lett.* **2002**, *89*, 126104.
(9) Lorente, N.; Persson, M. *Phys. Rev. Lett.* **2000**, *85*, 2997−3000.
(10) Lorente, N.; Persson, M.; Lauhon, L. J.; Ho, W. *Phys. Rev. Lett.* **2001**, *86*, 2593−2596.
(11) Bocquet, M.-L.; Lesnard, H.; Lorente, N. *Phys. Rev. Lett.* **2006**, *96*, 096101.
(12) Bocquet, M.-L.; Loffreda, D. *J. Am. Chem. Soc.* **2005**, *127*, 17207−17215.
(13) Lauhon, L. J.; Ho, W. *J. Phys. Chem. A* **2000**, *104*, 2463−2467.
(14) Komeda, T.; Kim, Y.; Sainoo, Y.; Kawai, M. J. *Chem. Phys.* **2004**, *120*, 5347−5352.
(15) Lee, J.-G.; Ahner, J.; Yates, J. T. *J. Chem. Phys.* **2001**, *114*, 1414−1419.
(16) Mate, C.; Somorjai, G.; Tom, H.; Zhu, X.; Shen, Y. *J. Chem. Phys.* **1988**, *88*, 441−450.

10.1021/ja067442g CCC: $37.00

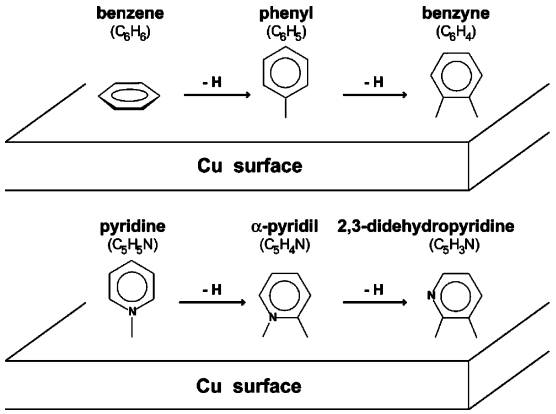

Figure 1. Successive dehydrogenation reactions of benzene (top) and pyridine (bottom) upon adsorption on a Cu surface as initiated by tunneling electrons.

these molecules adopt different conformations on metal surfaces: benzene lies flat, whereas pyridine is linked to the metal through the nitrogen atom in a perpendicular orientation as depicted in Figure 1. These different adsorption configurations may lead to different dehydrogenation reactions. Indeed, the initial assignment of the dehydrogenation products of benzene was C_6H_4 and that of pyridine was α-C_5H_4N[13] which implies double and single H scission, respectively. However, recent calculations[11] show that the STM dehydrogenation of benzene produces C_6H_5, indicating that, finally, benzene and pyridine dehydrogenation may share similar processes under an STM pulse. The first aim of this theoretical study is to rationalize the difference between benzene and pyridine with respect to the dehydrogenation process and final products. However, the main motivation of this study is to shed light onto STM-induced reactions on surfaces.

We thus report on DFT calculations of successive dehydrogenation pathways starting from both, adsorbed benzene and pyridine molecules. It is of especial interest to compare the experimental thresholds to the calculated activation barriers. The analysis of the different stages along the reaction pathway enables us to identify the electronic processes leading to dehydrogenation. We further perform IETS simulations on benzene, pyridine, and dehydrogenated fragments and compared them with the experimental results. From here we identify α-pyridil (α-C_5H_4N) as the dehydrogenation product of pyridine. We analyze our findings in terms of molecular conformation and electronic structure. This permits us to understand why phenyl, pyridine, and α-pyridil present tunneling-active C−H stretch modes while benzene does not.

2. Methodology

In this section, we present the ensemble of theoretical tools used in this study. The electronic structure calculations are performed using DFT within the generalized gradient approximation as implemented in the VASP code.[25] The electron−ion interaction is described by the projector-augmented wave (PAW) scheme,[26] and the electronic wave functions are expanded by plane waves up to a kinetic energy of 400 eV. The Cu(100) surface is modeled within the supercell approach by periodically repeated slabs. Each supercell contains four atomic layers of copper plus the adsorbed molecule and a vacuum region around 15 Å. The calculations are performed with the theoretical Cu lattice constant of 3.65 Å using a p(4 × 4) surface periodicity. We use a k-point set with 16 points in the surface Brillouin zone. The uppermost two copper layers as well as the molecular degrees of freedom are allowed to relax until atomic forces are lower than 0.01 eV/Å.

A delicate step in this computational work is the minimization of the reaction pathways and the search of intermediate stationary points or saddle points connecting the phase spaces of reactant and product. These saddle points are particularly relevant because they mark the moment when the system departs from a given structure to become something else; they are thus the transition states (TSs) of the reaction pathway. The climbing-image nudged elastic band (NEB)[27] implemented in VASP has been systematically used to find these saddle points along the adiabatic minimal energy pathway connecting each initial and final state of a given elementary step. Approximate structures of TSs are obtained with the minimization of a set of eight intermediate images.[28] To refine the TS geometry we have further minimized all the residual forces with a quasi-Newton algorithm. Finally, the TSs are identified by exhibiting the existence of a single normal mode associated with a pure imaginary frequency.[29] The corresponding soft mode lies in the reaction coordinate and gives fundamental information on the reaction pathway. The NEB method yields the globally optimal path rather than the locally restricted one and is thus more reliable than the constrained optimization method sometimes used for time-consuming reasons. In particular, the constrained optimization method may overestimate activation barriers as pointed out in a recent DFT study on water dissociation.[30]

An important part of this theoretical contribution is the analysis of the electronic structure in different configurations along the reaction pathways. Such studies permit the understanding of the electron-induced processes leading to the reactions. An important tool is the projected density of states (PDOS)[31] onto a molecular orbital, MO, as given by

$$\mathrm{PDOS}(E) = \sum_{\lambda} |\langle \mathrm{MO}|\lambda\rangle|^2 \, \delta(\epsilon_\lambda - E) \qquad (1)$$

where λ are the labels of the eigenenergies, ϵ_λ, and eigenstates, $|\lambda\rangle$, of the chemisorbed system and MO is the free-molecule state onto which the density of states is projected. The MO is calculated for the free molecule distorted to its chemisorption geometry. The PDOS is informative of the molecular character of the chemisorbed system. From this point of view, it is more interesting than the PDOS on atomic orbitals used in many works on molecular adsorption because it uses the molecular orbitals as analyzing building blocks of the system's electronic structure.

Next, the modes of the stable relaxed structures are evaluated by diagonalization of the dynamical matrix. This matrix is obtained by a finite-difference method implemented in VASP. In this vibrational

(17) Giessel, T.; Schaff, O.; Lindsay, R.; Baumgärtel, P.; Polcik, M.; Bradshaw, A.; Koebbel, A.; McCabe, T.; Bridge, M.; Lloyd, D. R.; Woodruff, D. P. *J. Chem. Phys.* **1999**, *110*, 9666−9672.
(18) Dougherty, D.; Lee, J.; Yates, J. *J. Phys. Chem. B* **2006**, *110*, 11991−11996.
(19) Hahn, J. R.; Ho, W. *J. Chem. Phys.* **2006**, *124*, 204708.
(20) Weinelt, M.; Wassdahl, N.; Wiell, T.; Karis, O.; Hasselström, J.; Bennich, P.; Nilsson, A.; Stöhr, J.; Samant, M. *Phys. Rev. B* **1998**, *58*, 7351−7360.
(21) Doering, M.; Rust, H.-P.; Briner, B.; Bradshaw, A. *Surf. Sci.* **1998**, *410*, L736−L740.
(22) Pascual, J. I.; Jackiw, J.; Song, Z.; Weiss, P.; Conrad, H.; Rust, H.-P. *Surf. Sci.* **2002**, *502*−*503*, 1−6.
(23) Bilić, A.; Reimers, J.; Hush, N. *J. Phys. Chem. B* **2002**, *106*, 6740−6747.
(24) Morin, C.; Simon, D.; Sautet, P. *J. Phys. Chem. B* **2003**, *107*, 2995−3002.
(25) Kresse, G.; Fürthmuller, J. *Comput. Mater. Sci.* **1996**, *6*, 15.
(26) Kresse, G.; Joubert, D. *Phys. Rev. B* **1999**, *59*, 1758−1775.
(27) Henkelman, G.; Uberuaga, B.; Jonsson, H. *J. Chem. Phys.* **2000**, *113*, 9901−9904.
(28) It should be noted that the pathway minimization procedure is performed at the gamma point only. However, all intermediate or transition states described in the figures result from further geometry optimization with the finer (4 × 4 × 1) k-point grid.
(29) A mode frequency is a measure of the curvature of the PES. In the case of an imaginary frequency, the PES has turned from concave to convex revealing the appearance of a saddle point and hence characterizing the TS. The larger the modulus of the imaginary frequency, the steeper the descent along the reaction coordinate.
(30) Meng, S.; Wang, E.; Frischkorn, C.; Wolf, M.; Gao, S. *Chem. Phys. Lett.* **2005**, *402*, 384−388.
(31) Hoffmann, R. *Rev. Mod. Phys.* **1988**, *60*, 601−628.

analysis, only the degrees of freedom of the relaxed adsorbate are considered (molecular vibrations) because we are interested in IETS signals of high frequency (C−H stretch frequencies) that are little perturbed by the low-frequency modes originating from surface phonons. Finally, IETS simulations are performed with a many-body extension of the Tersoff−Hamman theory[32] used for the STM[9,11] simulations. For a detailed description of the theory, please see ref 33.

3. Adsorption Properties

First, we briefly present the results of a systematic adsorption study of benzene and pyridine on Cu(100) in order to exhibit possible metastable sites which may be important for the pathway analysis.

Three high-symmetric flat adsorption configurations are found for adsorbed benzene with decreasing chemisorption energies: fourfold hollow (chemisorption energy of −0.3 eV), bridge (−0.2 eV), and top (−0.1 eV) sites. Previous studies[34] have yielded an adsorption energy of −0.68 eV.[35] These results consistently show that benzene is weakly adsorbed over the highest coordinated site on Cu(100) at a bonding distance of 2.3 Å. Due to the small involved energy barriers, in-plane rotation and diffusion processes on the surface are likely to occur. The adsorption of benzene also induces a weak sp^3 hybridization including an expansion of the carbon ring from 1.40 Å to 1.42 Å and an out-of-plane tilt of H atoms about 9°.[11,34] Very similar results and discussion are also presented in ref 38.

Experimental adsorption data are available on Cu(111)[39,40] and on Cu(110).[41] On Cu(111), the adsorption energy estimated from a 225 K desorption temperature corresponds to an adsorption energy of −0.429 eV,[39] while, on Cu(110), the desorption temperature is rather 280 K.[41] On both surfaces the molecule lies flat at low coverages, in agreement with our calculations. The Cu(100) surface, the object of the present study, is expected to have very similar behavior, somewhat intermediate between those of Cu(111) and Cu(110).

In contrast to benzene, pyridine's molecular plane can be tilted with respect to the surface. Indeed, the minimum-energy conformation corresponds to a pyridine molecule with a perpendicular orientation on top of a single Cu atom and a yaw angle of 45° aligning the molecular plane along the diagonal of the square unit cell. The corresponding chemisorption energy is −0.7 eV with a bonding N−Cu distance of 2.03 Å. The potential energy surface is more corrugated than the benzene one, since the pyridine chemisorption energy drops to −0.1 eV on a fourfold site. Hence, benzene and pyridine behave differently in contact with a metal surface. However, the adsorption energy of a pyridine molecule with its plane parallel to the surface such as the conformation found in solution[42] almost equals the adsorption energy of benzene. The in vacuum experimental data in the low-coverage case are available on the Cu(110) surface.[15] The adsorption energy estimated from first-order desorption spectra is −0.97 eV. The conformation of the molecule corresponds well with the above theoretical geometry.[15]

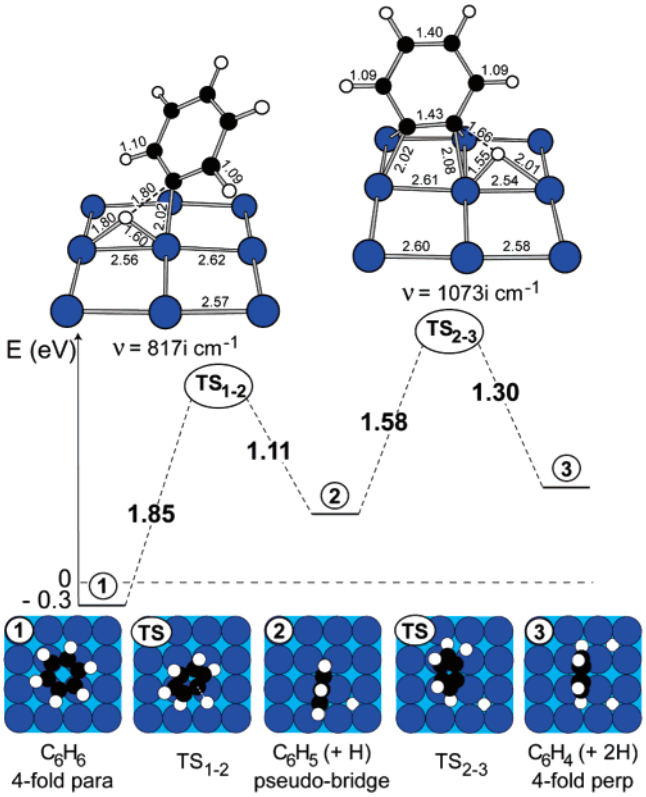

Figure 2. Energy profile for the successive dehydrogenation of C_6H_6 on Cu(100) with respect to the sum of energies of the free benzene molecule and the relaxed Cu(100) surface. The geometrical structures of the transition states are given in the top panel with bonding distances in Å and with the imaginary frequency of the soft mode at the reaction coordinate, which corresponds to a weakening C−H stretch mode (dotted line). Top views of all states along the reactive profile are given in the lower panels with the symmetry of their adsorption site.

4. Reaction Pathways

The reaction pathways are studied by evaluating the adiabatic barriers to successive dehydrogenation steps of benzene and pydirine. Since it is fundamental to characterize the initial and final stages of each dehydrogenation process, the adsorption of the dehydrogenation products has also been investigated.

4.1. Benzene Dehydrogenation. In the case of benzene, the first hydrogen scission leads to a phenyl radical C_6H_5 and the second one leads to the benzyne species, C_6H_4. As previously found,[11] both dehydrogenation products stand upright on the surface at bridge and hollow sites, respectively, for C_6H_5 and C_6H_4, panels 2 and 3 of Figure 2. For the two endothermic steps, each TS is determined by an NEB calculation followed by a thorough vibrational analysis of the TS. The TS geometry and imaginary frequency are provided in the top panel of Figure 2.

(32) Tersoff, J.; Hamman, D. R. *Phys. Rev. Lett.* **1983**, *50*, 1998−2001.
(33) Lorente, N. *Appl. Phys. A* **2004**, *78*, 799−806.
(34) Lorente, N.; Hedouin, M. F. G.; Palmer, R. E.; Persson, M. *Phys. Rev. B* **2003**, *68*, 155401.
(35) Both calculations have been performed in two different implementations of DFT (VASP [ref 25] here, DACAPO [ref 36] in ref 34), and despite performing the calculations in the same numerical conditions there is a sizable energy difference probably stemming from the actual implementation of DFT in each code [ref 36].
(36) http://dcwww.fysik.dtu.dk/campos/Dacapo/download.html.
(37) In particular the VASP calculations used PAW while the DACAPO ones were performed with ultrasoft pseudopotentials; see ref 26 and references there in.
(38) Bilić, A.; Reimers, J. R.; Hush, N. S.; Hoft, R. C.; Ford, M. J. *J. Chem. Theory Comput.* **2006**, *2*, 1093−1105.
(39) Xi, M.; Yang, M. X.; Jo, S. K.; Bent, B. E.; Stevens, P. *J. Chem. Phys.* **1994**, *101*, 9122−9131.
(40) Lukes, S.; Vollmex, S.; Witte, G.; Wöll, G. *J. Chem. Phys.* **2001**, *114*, 10123−10130.
(41) Lomas, J. R.; Baddeley, C. J.; Tikhov, M. S.; Lambert, R. M.; *Langmuir* **1995**, *11*, 3048−3053.
(42) Wan, L.-J.; Wang, C.; Bai, C.-I.; Osawa, M. *J. Phys. Chem. B* **2001**, *105*, 8399−8402.

The imaginary frequencies correspond to softmodes revealing the appearance of a saddle point and hence characterizing the TS. In the reactions analyzed here, the reaction coordinates correspond to a stretch mode of a loose C−H bond as marked by dotted lines in the top panel of Figure 2. Notably, the TS_{1-2} and TS_{2-3} geometries, Figure 2, exhibit similar atomic positions for the breaking σ bond. The loose C−H bond is actually involved in a three-membered metallacycle Cu−C−H. In other words, C and H atoms share almost the same on top adsorption site,[43] as previously observed for the reverse hydrogenation mechanism.[44] This similarity between the geometrical structures of TS_{1-2} and TS_{2-3} is in apparent contradiction with different activation energies: the first dehydrogenation step costs almost 0.3 eV more than the second step. This energy difference corresponds to the adsorption energy of the benzene molecule. Indeed, in order to react, the benzene molecule first desorbs and almost aligns its molecular plane with the surface normal while pointing one C−H bond toward one single metal atom. As a result, this transient upright benzene and the phenyl radical react similarly regarding the dehydrogenation reaction: their hydrogen scission intrinsically costs ~1.5 eV. This quantity agrees with estimates based on the dehydrogenation of benzene on Cu(110).[14] However, the calculated gas-phase dehydrogenation barrier is 4.5 eV.[45] This large energy difference between the gas and chemisorbed phases is due to the attractive interaction between the reaction products and the metallic surface.

The experiments on STM-induced dehydrogenation find a reaction threshold at 2.9 V on Cu(100)[13] or 2.4 V on Cu(110),[14] the difference probably stemming from the measuring method rather than from physical properties.[14] At 1.5 V, the molecule would hop away from its original site, but no C−H fragmentation could be observed.[13] These data are in good agreement with the adiabatic barriers of Figure 2 because breaking the C−H bond globally costs 1.85 eV, but the molecule can already desorb at 1.5 eV. The threshold to the TS_{1-2} state is well below the experimental 2.4 V needed to dehydrogenate the molecules. Hence, at 1.5 V the only possible reaction is desorption, while at 2.4 V dehydrogenation is possible.

As discussed in ref 14, our calculations confirm that the 2.4 eV onset is not connected with the activation barrier for the C−H bond breaking. The minimum energy required to traverse both the TS_{1-2} and TS_{2-3} transition states in a single step is 2.32 eV, but if the crossing of the first transition state dissipates all of its minimum excess energy through the recoil of its departing hydrogen atom, then an additional 1.11 eV of energy, making 3.43 eV total, would be required. Hence detailed knowledge of the reaction dynamics must be obtained before accurate estimates of the actual threshold energy can be made.

4.2. Pyridine Dehydrogenation. The double dehydrogenation of pyridine is presented in Figure 3. The product of the pyridine dehydrogenation corresponds to H scission from one of the two adjacent α positions relative to the nitrogen atom (see lower panel 3 of Figure 3). Further dehydrogenation of this α-pyridil C_5H_4N fragment yields a 2,3-didehydropyridine C_5H_3N fragment (see lower panel 4 of Figure 3) where the second removed hydrogen lies in a β position relative to the nitrogen atom. In this final state, the nitrogen atom is not directly bound to the metal surface anymore.

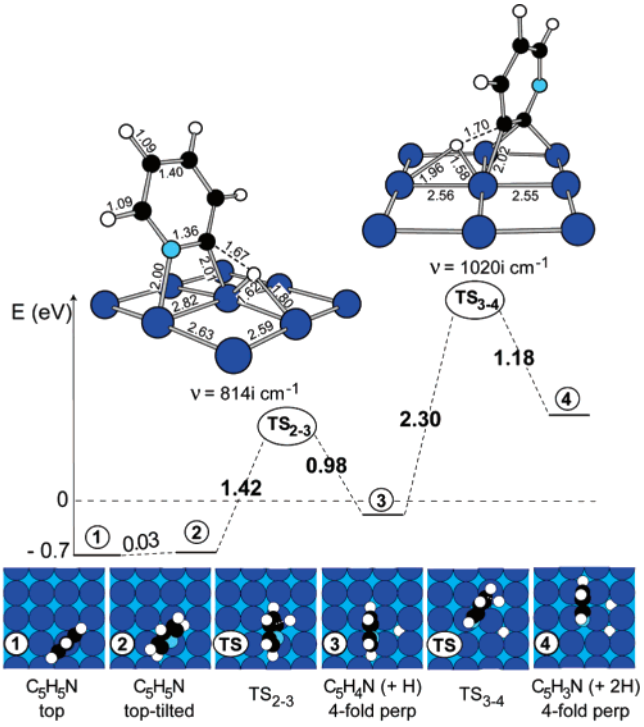

Figure 3. Energy profile for the successive dehydrogenation of C_5H_5N on Cu(100). Nitrogen atoms are depicted in blue. See caption of Figure 2 for additional information.

Optimized structures of the TS show similarities with the previous TS for benzene. Both carbon and hydrogen atoms of the breaking C−H bond are mainly in interaction with the same copper atom with bonding distances of about 2 Å and 1.6 Å, respectively. The bond breaking C−H distance is about 1.70 Å as in the benzene case. However, there are some subtle differences: the loose C−H lies in the plane of the TS_{1-2} and the TS_{2-3} of benzene, whereas the abstracted H is clearly out of plane for TS_{2-3} and TS_{3-4} of pyridine. This is due to the different molecular site of the TS: in the case of benzene, the TS tends to occupy hollow or near hollow sites, while, in the pyridine case, the molecular fragment is rather aligned onto a bridge site. The closest available site for H adsorption is thus pushed outside the molecular plane in the pyridine case. The imaginary frequencies of the TS are very close to the ones in the benzene, showing the locality of the C−H interactions during the dehydrogenation process.

Despite the above similarities both endothermic pathways display different barriers: 1.42 eV for the dehydrogenation of pyridine and 2.3 eV for the dehydrogenation of the α-pyridil fragment. This difference can be traced back to the adsorption configuration of the molecule in the initial and intermediate states. In the pyridine case, the molecule rotates, leaving intact the main N−Cu bond. However, from the vibrational analysis, we conclude that the energies to remove an H-atom are very similar in both types of molecules. The more acidic C−H close to the nitrogen atom presents a lower dissociation barrier favoring α-pyridil fragments due to the electronegativity of the neighboring nitrogen atom. This is also the case for phenyl dehydrogenation, where the dangling bond of the carbon atom

(43) The separating H rather lies in a pseudo-bridge position than in a strict on top position.
(44) Loffreda, D.; Delbecq, F.; Vigné, F.; Sautet, P. *J. Am. Chem. Soc.* **2006**, *128*, 1316−1323.
(45) Erwin, K. M.; DeTuri, V. F. *J. Phys.Chem. A* **2002**, *106*, 9947−9956.

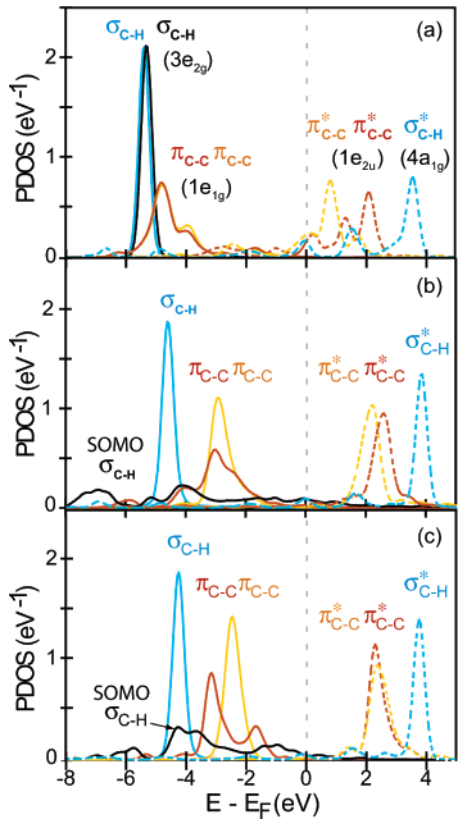

Figure 4. Projected density of states (PDOS) onto the frontier molecular orbitals of the full C_6H_6/Cu(100) (a), of the TS_{1-2} of Figure 2 (b), and C_6H_5/Cu(100) (c) systems. The reference molecular orbital on which the density of states of the full system is projected, eq 1, is signaled on each curve. For C_6H_6/Cu(100) we find the HOMO ($1e_{1g}$ for the free molecule that is a π_{C-C} orbital) substantially broadened by the interaction with the copper d-band, the LUMO ($1e_{2u}$ or π^*_{C-C}), and other molecular orbitals that are also perturbed by the interaction with the substrate. For the dehydrogenation process it is interesting to follow the evolution of the $3e_{2g}$ or σ_{C-H} orbitals. In (a) the PDOSs of the σ_{C-H} orbitals are sharp lorentzians, reflecting the small hybridization with metallic orbitals. In (b) one of the orbitals survives, while the other one (SOMO) becomes extremely broadened, showing its large interaction with the metal. In (c) there is a remaining low-energy σ_{C-H} peak, while the SOMO is almost as broadened as in (b).

induces a lower barrier in the adjacent C−H bonds. From our calculations, we estimate that the presence of nitrogen in pyridine reduces the intrinsic dehydrogenation energy by ~0.1 eV as compared to the total C−H scission energy of ~1.5 eV found for benzene; see above.

Finally, we cannot rule out double dehydrogenation of pyridine based on energetic arguments alone. Even if the adiabatic barrier of double dehydrogenation is 3.72 eV, a nonadiabatic estimate, like the one for the benzene dehydrogenation (see above), would yield a 2.74 eV barrier while the experimental STM threshold is 2.9 eV.[13] In order to determine the product of an STM induced dehydrogenation, the analysis of the IETS data is necessary.[11]

5. Electron-Induced H Detachment

From the study of the electronic structure at the different TSs in the reaction pathway, we can extract information about the actual process that leads to H dissociation under an STM pulse. In the case of benzene, Figure 4 shows the evolution of the electronic structure from the chemisorbed benzene molecule (a), to the chemisorbed phenyl fragment (c), and passing by the TS_{1-2} (b).

The electronic structure of benzene has been analyzed in ref 34. In Figure 4a, we find the same features as those in ref 34. The interaction of the HOMO, π_{C-C}, with the substrate is larger[34] and basically taking place with the Cu d-band. The LUMO, π^*_{C-C}, are somewhat broadened and split with some small electron occupation, showing that charge transfer is small. For a complete description of the electronic structure of the C_6H_6/Cu (100) system, please refer to ref 34.

The electronic configuration of the TS_{1-2}, Figure 4b, shows the adiabatic evolution of the electronic structure in an intermediate stage of the dehydrogenation process. The effect of removing one H leads to the creation of a phenyl fragment. We have chosen the electronic structure of this phenyl fragment in order to project the wavefunctions of the full system at the TS_{1-2}. Hence the PDOS resembles that of Figure 4c. Hence, we discuss the phenyl PDOS first, Figure 4c.

In the case of the phenyl system, we find that one of the two σ_{C-H} orbitals has been seriously distorted by the removal of one H.[34] The new orbital is the singly occupied molecular orbital (SOMO) of the phenyl fragment, and it accommodates a large fraction of a substrate electron. The interaction of this orbital with the substrate is very enhanced, leading to an important rehybridization with metallic states. This leads to a PDOS feature that extends over the Cu band, Figure 4c. The doubly degeneracy of the π_{C-C} system for benzene is also strongly perturbed by the removal of one H atom, and we see the different behavior of the PDOS depending on which of the two π_{C-C} orbitals the density of states is projected. Indeed, one peak is much sharper than the other one, showing that it is basically ignorant of the presence of the metal.

The main difference between the cases corresponding to Figure 4b and c is the fragment conformation with respect to the substrate. Indeed, the SOMO is very perturbed by the presence of the surface in the transition state, Figure 4b, and it extends over 10 eV about the Fermi energy. As we have just seen, the character of this orbital is basically σ_{C-H}, implying that charge redistribution during the dehydrogenation process will necessarily affect the C−H bonds. However, there is a component of π^* character. This means that the SOMO at the TS_{1-2} can efficiently mix the states originating from the π^*_{C-C} system with the σ_{C-H} electronic structure.

These results permit us to reach several conclusions on the actual STM-induced dehydrogenation process. As discussed in ref 14, the energy barrier is neither associated to the actual activation barrier of H scission (see section 4.1) nor associated with a given electronic resonance on the σ^*_{C-H} orbital. Indeed, this can be seen in Figure 4, where the electronic structure associated with the σ^*_{C-H} orbital is roughly 4 eV above the Fermi energy, well beyond the 2.4 eV[14] or 2.9 eV[13] found in the STM threshold bias.[46] Hence, at the experiment's bias voltage, the electron is injected in the π^*_{C-C} system of Figure 4. From the adiabatic reaction pathway, we know that the injected electron must first initiate the desorption of the benzene molecule. This is likely achieved by excitation of the center of mass vibrations of the molecule. During the motion of the molecule, there is a large probability that part of the excess

(46) One word of caution should be said whenever using energy values of the electronic structure obtained from Kohn and Sham orbitals of a DFT calculation: typically electronic energies are undervalued, so the above orbitals are probably further away from the Fermi level than the peaks depicted in Figure 4.

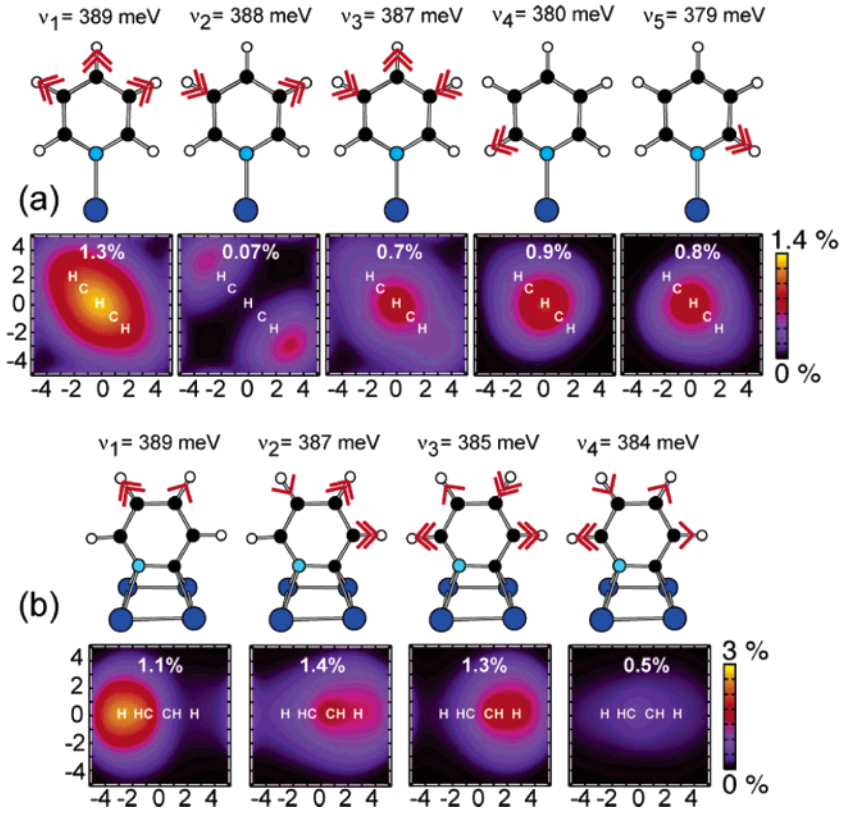

Figure 5. Sketch of all C−H stretch modes (frequencies included in meV) for adsorbed pyridine (a) and α-pyridil (b) molecules and their theoretical inelastic efficiencies over the p(4 × 4) unit cell of Cu(100) (10.32 Å × 10.32 Å). The computed relative change in conductance at the center of the unit cell is included in percent for each vibration mode.

electron energy is redistributed to other degrees of freedom. This will trigger one H dissociation. At TS_{1-2} the σ and π^* are efficiently coupled; hence the electron can relax from π^* to the σ orbitals by yielding its energy to vibrational excitation and eventually to the rupture of the C−H bond. Finally, the metal substrate equilibrates the system by damping out the excess electron and vibrational energies. This process is severly limited by the negative ion lifetime that lies in the femtosecond time scale, leading to very low yields.[14]

6. IETS of Pyridine and α-Pyridil

The scanning possibilities of the STM permit us to record the inelastic signal above the molecular region and to create IETS maps. In Figure 5 we show the results of our IETS map simulations for adsorbed pyridine (a) and α-pyridil (b). The simulations calculate the relative change in conductance due to the opening of the inelastic channel; by repeating the calculation over the molecular area, the IETS map is obtained for each mode (see refs 9 and 46).

The upper panel of Figure 5 shows the frequencies and eigenvectors of the C−H stretch modes for pyridine. The frequencies can be divided in two degenerate modes at 380 meV (379 and 380 meV in our simulation) and three degenerate modes at 388 meV (387, 388, and 389 meV). These two sets are localized in the lower (380 meV) and upper (388 meV) H atoms, showing that the bond strength is not the same for these two sets of C−H bonds. This behavior was also found for phenyl (see ref 11), but the energy split was 20 meV rather than 10 meV here. This shows that chemisorbed pyridine is less asymmetric than phenyl which can be understood by the large electron affinity of this latter fragment. Indeed, the PDOSs on the frontier orbitals of both molecules show this behavior: while phenyl presents a large capture of electrons from the metal, by producing a long SOMO tail below the Fermi level, Figure 4c, pyridine, Figure 7, shows a minor HOMO tail above the Fermi level, indicating small donation to the metal surface.

The IETS maps show variations in conductance in good agreement with the symmetry of the mode and of the electronic structure at the Fermi level. In Figure 7 we see that the main molecular electronic structure at the Fermi level displaying a partial σ_{C-H} character is given by the HOMO. Pyridine's HOMO is totally symmetric with respect to the two symmetry planes in the C_{2v} point group of the molecule−surface system. Hence, the nonzero matrix elements entering the electron-vibration coupling[10,11] are the ones coupling to electronic states that have the same symmetry as the vibrational mode. These states are the ones that are responsible for the IETS map.[10,11,47]

The dehydrogenated fragment, α-pyridil, has a lower symmetry as can be seen in the sketches of Figure 5b. Here charge transfer affects equally all C−H bonds, and the C−H stretch modes are basically degenerate. Indeed, the maximum change in frequencies is 5 meV. The lower symmetry of the modes translates into the IETS maps: the variations in conductance over α-pyridil are not centered on the molecule. Instead, the maximum of the IETS signal is systematically shifted to one side of the molecule, depending on the motion of the excited vibrational mode.

(47) Lorente, N.; Rurali, R.; Tang, H. *J. Phys.: Condens. Matter* **2005**, *17*, S1049−S1075.

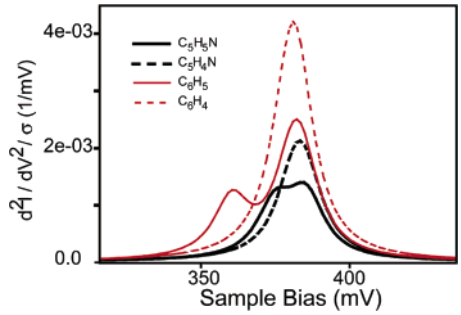

Figure 6. Simulated IETS spectra of C_5H_5N, C_5H_4N, C_6H_5, and C_6H_4: change of conductance as a function of the tip−surface bias voltage above the center of each fragment. The spectra have been convoluted with a 14-meV wide Lorentzian in order to simulate the experimental broadening.[7] Each Lorentzian, has been centered at the modes of Figure 5.

Table 1. Comparison between Theory and Experiment[13] of the Change in Conductance in % over the Center of the Molecule for Four Different Molecules Chemisorbed on Cu(100)

molecule	experiment	theory
C_6H_5	5%	4.3%
C_6H_4	-	8.3%
C_5NH_5	5%	3.7%
C_5NH_4	4%	3.9%

On each of the IETS maps of Figure 5, the relative change in conductance about the molecular center is displayed. This relative change is the surface of each spectral peak given in Figure 6. Figure 6 is the d^2I/dV^2 normalized to the elastic conductance when the STM tip is located on top of the molecular center and can be compared with the IETS spectra of ref 13. In the same figure, the IETS spectra for C_6H_5 and C_6H_4 are depicted.[11] We remark that the C_6H_5 signal is larger than the IETS signal for C_5H_5N. Indeed, the overall change in conductance about the molecular center is 4.3% for phenyl while it is 3.7% for pyridine, Table 1. This difference can be traced back to the type of molecular bonding with the surface: in phenyl the SOMO strides the Fermi energy due to the large donation from the susbtrate, Figure 4c; in pyridine, the analogue HOMO has now a small representation at the Fermi level, as a consequence of the dative bond due to the nitrogen lone pair. Then tunneling electrons couple more easily with the C−H stretch vibration in phenyl than in pyridine. Experimentally, the change of conductance is roughly the same for pyridine (5%) as it is for phenyl (5%).[13] See Table 1 for a comparison of experimental and theoretical values. However, there are a series of experimental parameters that may affect this result and are not included in the simulation, such as the tip state. In the experimental work[13] the tips were not the same. Hence, our results are probably within the experimental error bar.

Another interesting feature of Figure 5 is the spectral shape. The dehydrogenated species, C_6H_4 and C_5H_4N, present a unique peak while phenyl and pyridine show two maxima. This is a consequence of the frequency splitting in both types of molecules as discussed above. In the case of pyridine the splitting is only of ∼10 meV. In the case of substantial experimental broadening, only one peak may be resolvable as the experimental spectra of ref 13 show. The experimental work argues on the formation of α-pyridil after the STM pulse.[13] They find a 4% change in conductance as well as a 3-meV shift of the peak of α-pyridil above the pyridine peak. We find a 3.9% change in conductance and a peak shift, if we assumed that the double peak of pyridine, Figure 5, is broadened into one peak. In this case, we find a 3-meV peak shift in excellent agreement with the experiment. From this analysis we conclude that the STM-induced dehydrogenation of ref 13 led to α-pyridil formation.

Recent experiments on IETS in pyridine on Ag(110)[19] show a single peak roughly at the same energy. The change in conductance is 3.8%. It is difficult to say whether the difference with the 5% found on Cu(100) is significative, but it is in agreement with the above analysis that the IETS strength depends on the amount of charge transfer involving orbitals that are active in the studied vibration. Silver is less reactive than copper, which translates into less hybridization and smaller charge transfers.

The actual molecular conformation is important in order to excite the vibration. As we can see in the IETS maps, certain modes can be excited by placing the STM tip on certain positions of the molecule where other modes cannot be excited. However, tunneling-active modes arise from molecular electronic structure at the Fermi level that leads to nonzero matrix elements of the electron−vibration interaction, rather than from geometrical conformation effects. As discussed in ref 11, the fact that benzene presents no tunneling-active mode, while C_6H_5 and C_5H_5N do, is not due to the upright position of the molecule as claimed in ref 19 but to the fact that there is a substantial molecular electronic structure with C−H character at the Fermi level as explained above for adsorbed phenyl and pyridine. Conversely, benzene basically has π_{C-C} character at the Fermi energy, Figure 4a. Hence, in the case of phenyl and pyridine, the tunneling electron will be injected directly in the C−H bonds leading to a sizable change in conductance for the C−H stretch vibrations and in the C−C bonds for benzene with little coupling with the C−H stretch modes.

7. Conclusions

We have presented simulations and theoretical work on the dehydrogenation of benzene and pyridine molecules on Cu(100) under an STM pulse motivated by the experimental results of refs 13 and 14. We made use of the NEB method[27] to find activation barriers and transition states. This pathway study, combined with the evaluation of the electronic structure at different steps of the dehydrogenation, provides a consistent picture of the STM-induced reaction.

We find that the scission of a C−H bond is a local process being basically the same for benzene and pyridine. This statement is based on the similar values of the energy needed to break the C−H bond, roughly 1.5 eV, and on the very similar imaginary frequencies of the transition states. Nevertheless, the adiabatic pathway reveals an important difference: benzene is largely desorbed during the dehydrogenation process while pyridine pivots on the N−Cu axis. Hence, more energy is needed for the first dehydrogenation barrier of benzene. In the case of pyridine, we find the preference of α hydrogen scission due to the larger electronegativity of nitrogen as compared to carbon.

The study of the electronic structure along the pathway allows us to propose an electron-induced dehydrogenation mechanism. The STM injects an electron in the π^*_{C-C} electronic structure, which induces motion of the benzene molecule. During this evolution, the transition state is formed where σ and π^* states are efficiently mixed, permitting the rupture of the C−H bond

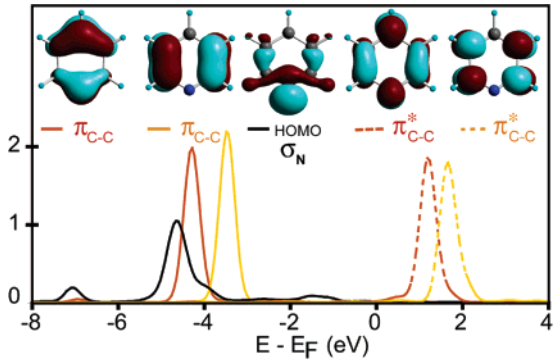

Figure 7. Projected density of states (PDOS) of C_5H_5N/Cu(100) on the frontier orbitals of C_5H_5N. The low-lying peak is the PDOS on the HOMO of the isolated pyridine. The HOMO is depicted above and has a σ_{C-H} and nitrogen lone pair characters. This pyridine orbital resembles the SOMO of the isolated phenyl fragment, Figure 4c. Upon adsorption the pyridine HOMO is shifted below the π_{C-C} orbitals reflecting the small electron donation from the molecule to the metal.

by vibrational excitation. Hence the initial electron ends up populating the σ_{C-H} electronic structure. The energy lost by breaking this bond is compensated by the energy gained in the electronic relaxation from the initial π^*_{C-C} state to the SOMO of the forming phenyl.

From our adiabatic studies, double dehydrogenation of benzene or pyridine seems out of reach at the actual experimental voltages. However, nonadiabatic processes cannot be discarded, and our pathway study cannot conclude on the possibility of double dehydrogenation. In order to identify the final dehydrogenation product we need to compare our IETS simulations with the experimental data.

Our simulations agree with the existing IETS data on benzene, pyridine, and dehydrogenation fragments, allowing us to identify phenyl as the benzene dehydrogenation product[11] and α-pyridil as the pyridine dehydrogenation product. Eventually, our calculations permit us to understand the tunneling active modes. In particular, the absence of IETS signals from C−H stretch modes of benzene has been rationalized by the absence of σ_{C-H} electronic structure at the Fermi energy of the benzene−surface complex. Benzene dehydrogenation broadens one σ_{C-H} orbital up to the Fermi level, implying a direct coupling of the injected electron with the C−H bond. Hence, vibrational excitation becomes efficient. Pyridine similarly presents a small charge depletion from its HOMO (σ_{C-H}) to the metal (Figure 7), yielding a weaker electron−vibration coupling. From our IETS simulation, we infer that the upright position of the molecule, and, in general, its conformation, plays a minor role except in the spatial distribution of the IETS signal. The IETS signal distribution is a direct consequence of the electronic symmetry at the Fermi level in combination with the mode symmetry.[10,11] Hence, IETS yields information not only on the vibrational properties of the adsorbed molecule but also on its electronic properties.

Acknowledgment. This work has been partially supported by ANR *Jeunes Chercheurs* INESS. We thank CALMIP, IDRIS, and CINES (CNRS, France) for CPU time and assistance.

Supporting Information Available: Absolute energies (in hartree) and optimized geometries of the different conformations of this work. This material is available free of charge via the Internet at http://pubs.acs.org.

JA067442G